Journal of Materials Chemistry A

Freeze-Extrusion for Controllable Assembly of 3-Dimensional Ultra-Fine and Amorphous Fibrous Matrices: Potential Applications in Sorption

Journal:	*Journal of Materials Chemistry A*
Manuscript ID	TA-ART-02-2018-001845.R2
Article Type:	Paper
Date Submitted by the Author:	26-Apr-2018

Complete List of Authors:	Mu, Bingnan; University of Nebraska-Lincoln College of Education and Human Sciences, Li, Wei; University of Nebraska-Lincoln, Textiles Xu, Helan; university of nebraska-lincoln, Textiles, Merchandising and Fashion Design Xu, Lan; university of nebraska-lincoln, Agronomy and Horticulture Yang, Yiqi; university of nebraska-lincoln, department of biological systems engineering

Journal of Materials Chemistry A

ARTICLE

Freeze-Extrusion for Controllable Assembly of 3-Dimensional Ultra-Fine and Amorphous Fibrous Matrices: Potential Applications in Sorption

Received 00th January 20xx,
Accepted 00th January 20xx

DOI: 10.1039/x0xx00000x

www.rsc.org/

Bingnan Mu[a], Wei Li[a], Helan Xu[a], Lan Xu[b] and Yiqi Yang[a,c,d,*]

This paper studies the formation mechanism, properties and applications of fibrous matrices via freeze-extrusion. Though some porous fibrous materials via freezing and freeze-drying have been developed, applications of these materials are limited due to the lack of comprehensive studies on the formation mechanism. We demonstrate that polymer continues its concentration, precipitation, and accumulation along the direction of the temperature gradient in gaps between ices before the formation of fibrous matrices. Fibers with branched structures in matrices from freeze-extrusion are continuous and have large amorphous areas. Alignments of fibers are controllable. Porosity of freeze-extruded fibrous matrices is as high as 99.93%. These properties endow such matrices with good mechanical properties and excellent performance in water treatment. Good mechanical properties of matrices ensure the reusablity in water treatments. Sorption capacities of these matrices on major water pollutants, such as textile dyes and organic solvents, are as high as 1200 mg/g and 34000%, respectively. Sorption capacities remain almost the same even after 50 times of reuses.

Introduction

Three-dimensional (3-D) fibrous matrices with large specific surface area have great potential to be applied in thermal conductivity,[1] sound absorption,[2] demulsification,[3] catalytic electrodes,[4] superhydrophobic coatings,[5] artificial muscles,[6] sensors[7] and tissue engineering.[8] Currently, there are three major approaches to develop 3-D fibers matrices: electrospinning, phase separation, and freeze-drying. Initially, electrospinning was used for fabricating two-dimensional (2-D) fibrous materials from bio-based[9] and synthetic polymers.[10] The alignments of fibers were controlled by rotating the grounded target. Applying surfactants or freeze-drying, 3-D fibrous matrices were developed by electrospinning. Adding surfactants into spinning dopes, zein, keratin and soy protein were electrospun into randomly oriented 3-D fibrous scaffolds.[11-13] However, such approach cannot precisely control the orientation of fibrous matrices. Some researchers[14, 15] made 3-D fibrous matrices by freeze-drying dispersions of chopped electrospun fibers (FDCE). However, these matrices would not have ideal mechanical properties due to short average fiber length (48 μm) and controlled alignments of fibers.[15] Phase separation is another approach to fabricate fibrous matrices. Based on this approach, Liu et al successfully developed Nano-Fibrous Poly(L-Lactic Acid) matrices.[16] However, only a limited number of polymers could be made into such matrices because not all dissolved polymers could go through gelation, which is the key process required in this method. More importantly, it is hard to control the fiber alignment in matrices. Morphologies of matrices after phase separation are ranging from fibers to flakes and there is no practical way to control such morphologies.[17]

Freezing combined with freeze-drying is another method to fabricate aligned 3-D porous matrices. The process is relatively simple. A polymer solution is first frozen in a cold bath and then freeze-dried via sublimation. Matrices developed could be fibrous,[18, 19] non-fibrous,[20] or contains both fibrous and non-fibrous structures.[21-23] However, reasons and conditions to have various structures in these matrices remain unknown. No studies on the formation mechanism of fibrous matrices have been launched except a few investigations on the formation of non-fibrous and aligned porous structures. In these investigations,[20, 24, 25] authors proposed a theory to explain the formation of their matrices. When ices are formed from solvents such as water and grow along with the temperature gradient, dissolved or suspended polymer is extruded from the growing ices and aggregates in the gaps between ices. Under such a temperature gradient, ices will form with a controlled direction. After all the solvents are converted to ices, removal of the orientated ice by freeze drying leads to the formation of 3-D aligned matrices. However, polymer particles or molecules are encapsulated in the ice if the rate of freezing is too fast. As a result, aligned matrices could not be formed by freezing and freeze drying. This theory partially explained the formation of

[a] Department of Textiles, Merchandising and Fashion Design, 234, HECO Building, University of Nebraska-Lincoln, Lincoln, NE 68583-0802, United States
[b] Department of Agronomy and Horticulture, University of Nebraska-Lincoln, Lincoln, NE 68583-0915, United States
[c] Department of Biological Systems Engineering, 234, HECO Building, University of Nebraska-Lincoln, Lincoln, NE 68583-0802, United States
[d] Nebraska Center for Materials and Nanoscience, 234, HECO Building, University of Nebraska-Lincoln, Lincoln, NE 68583-0802, United States
Electronic Supplementary Information (ESI) available. See DOI: 10.1039/x0xx00000x

3-D aligned fibrous matrices, but still cannot explain plenty of phenomena during their formation. For example, under different freezing rates, sizes of formed fibrous matrices are different. The size of matrices under low freezing rate is smaller than that under high freezing rate. Under the same freezing rate, density of fibrous matrices and diameter of fibers in matrices increase along the temperature gradient. Under the same freezing rate and polymer concentration, morphologies of matrices from various solvents are different. Some are fibrous matrices, and some are non-fibrous matrices. According to current theories, matrices sizes should not be affected by freezing rates, densities of matrices and diameters of fibers should be constant along with the temperature gradient. Morphologies of matrices using different solvents under same freezing rate and polymer concentration should be the same. Moreover, some phenomena were not considered by these mechanisms. For instance, according to our study, degree of crystallinity of fibers in matrices via freezing and freeze-dry is lower than those via other spinning methods, such as wet-spinning and electrospinning. Also, fibers have branched structures in these matrices. Currently, due to the lack of thorough understanding of the mechanism, development of fibrous matrices via freezing and freeze-drying has been rarely reported and applications of these matrices are limited.[22]

In this paper, we demonstrate the formation mechanism of 3-D ultra-fine fibrous matrices (UFMs) via freeze-extrusion, developed several UFMs with good mechanical properties, and investigated potential applications of these UFMs. Formation mechanism is proposed based on ice growth and solute precipitation, and then verified based on controlled fiber alignments and effects of polymer concentrations and freezing rates on diameters of fibers in UFMs. The properties and potential applications of UFMs made from polyacrylonitrile (PAN) and feather keratin have also been studied. These UFMs have continuous fibrous structures with large degree of amorphousness, controllable fiber alignments, tunable densities (as low as 0.65 mg/cm^3) and recoverable compressibility (up to 50 kPa). Based on the excellent properties described above, UFMs developed in this work can be potentially applied in water treatment.

Experimental

Materials

PAN, Polyvinyl alcohol (PVA) were purchased from JT Baker, Phillipsburg, NJ. PVA was made into UFMs to study the mechanism of fibrous matrices formation via freeze-extrusion. PAN was made into UFMs to remove oil from water and emulsions. Chicken feather barbs were provided by Featherfiber Corporation, Nixa, MO. Feathers were made into UFMs to remove dyes from water. Dimethyl sulfoxide (DMSO), chloroform, mineral oil, hexane and engine oils were purchased from VWR international, Bristol CT. DMSO was used to dissolve PAN while chloroform, mineral oil, hexane and engine oils were used to measure the solvent uptake of UFMs. Cysteine (98%) was purchased from EMD Chemicals Inc. Gibbstown, NJ. Urea (99.0%) was purchased from Oak Chemical, Inc. West Columbia, SC. Cysteine and urea were to dissolve keratin. The commercial dyes, CI Reactive Blue 19 (RB19), CI Reactive Black 5 (RB5) were purchased from Hoechst Celanese Corporation, Bridgewater, NJ, and used without further purification. Its purity was around 75% (desalt), which was determined by soxhlet extraction, and was used for calculations. RB 19 was used to dye PVA and RB5 was used to studied dye removal ability of UFMs since RB5 is a very common dye used in current textile industry and causes substantial pollution to the environment. Even traces of such dye in water lead to significant color change.

Study of mechanism of fibrous matrices formation

PVA was dissolved in water and DMSO to prepare PVA solution with concentrations of 0.2 and 0.5 g/L. These solutions were immediately cooled down to -20 and -80 ^{o}C by dipping the container into a coolant consisting of 50% (v/v) ethylene glycol/water. For easy observation of the formation of PVA fibrous matrices in solution during freeze extrusion, PVA was chemically reacted in an aqueous environment with RB19 at 0.5%based on the weight of PVA. Reaction scheme is shown in Scheme S1. The reaction between PVA and RB19 occurred in the presence of 100 g/L of sodium sulfate and 20g/L of sodium carbonate at 50 °C for 1 h with a PVA to water ratio of 1 to 20. After the chemical reaction, the unreacted and hydrolyzed dyes were completely removed from the colored PVA with water. Morphologies of the colored PVA during freezing were observed.

To control the alignments of fibers in PVA UFMs, cylinders of PVA solution were put into coolant in different manners. To make ice grow from rim to center of the solution, cylinders were put into coolant immediately to make sure all solution was surrounded by coolant. To make ice grow from bottom, cylinder of solution was lowered into coolant at a controlled rate of 2 mm/min. To make ice grow toward the center of sphere, a sphere container holding PVA solution was put into coolant immediately to ensure all solution was surrounded by coolant. Temperature of coolant was kept at -80 ^{o}C. After freezing, frozen solution was freeze-dried at -57 ^{o}C for 70 h.

Characterization of UFMs

UFMs Morphology

Morphological analysis of UFMs was studied using a scanning electron microscope (SEM, S3000N, Hitachi, Inc. Schaumburg, IL). Matrices were sputter-coated with gold/ palladium and observed at a voltage of 15 kV. Fiber diameters were measured using software Image J (National Institutes of Health, Bethesda, MD) by counting 100 fibers under each condition from their respective SEM pictures.

Wide angle X-ray diffraction measurement

This was used for the determination of degree of crystallinity of matrices and orientation of fibers in matrices. The diffraction patterns of fibers made by various methods were obtained by a Bruker D8 (Bruker, US) Discover model diffractometer equipped with an area detector and GAADS software. Fibers were mounted on a specially designed sample holder with the axis of the fibers

being perpendicular to the X-ray beam. A power of 40 kV and 30 mA were used during the X-ray measurements.

Compression test

This was to investigate durability and recoverability if UFMs in water treatments. Compression strength tests were carried out by TA XT Plus Texture Analyzer (Stable Microsystems Ltd, UK) equipped with two flat-surface compression stages and 10 N load cells.

Pore size and porosity measurement

Pore diameters were quantified using commercial software ImageJ (1.51v) from SEM images of UFMs. The porosity per unit volume was determined based on the standard method[15] for UFMs by Equation 1:

$$\eta = \frac{V_0 - m/\rho}{V_0} \quad \text{Equation.1}$$

where η is the porosity per unit volume, V_0 is the volume of the UFMs, m is the mass of the solid constituents, and ρ is the density of solid constituents. To quantify relationship between pore volume and sorption capacity, porosity per unit volume is converted to porosity per unit mass by Equation 2:

$$\varepsilon = \eta \frac{m}{\rho_0}\frac{1}{m} = \frac{\eta}{\rho_0} \quad \text{Equation. 2}$$

where ξ is the porosity per unit mass, ρ_o is the density of UFMs.

Determination of specific surface area

Sorption applications of UMFs were conducted under wet state and methylene blue sorption was used to measure the specific surface area of sorbents at swollen state. The surface area covered by one methylene blue molecule is typically assumed to be 130 $Å^2$ [26].

Applications of UFMs

Dye removal from water

Keratin barbs were used in this study because it is hydrophilic polymer and carries charges, which could sorb dyes in water via electrostatic force. Keratin UFMs were prepared first. Keratin solution was prepared according to the procedure developed by Xu et al.[27] Briefly, keratin was extracted by immersing 100 g chicken feather and 10 g cysteine into 1700 mL of 8 M urea aqueous solution with pH of 10.5 at 70 °C for 12 h. After centrifuge to remove undissolved residuals, the supernate was dialyzed with refreshed distilled water every 4 h for 36 h to remove urea and other salts. To increase the mechanical properties, chitin nanoparticles and oxidized sucrose were added into the protein supernate. Details procedures are shown in SI. The mixture was stirred for 5 min, kept at -20 and -80 °C in coolant for 2 h for freeze-extrusion and, finally, freeze-dried at -57 °C for 170 h. The freeze-dried keratin adsorbent was put into 70 °C oven for 1 h to allow the crosslinking reaction.

Measurement of sorption capacities of dyes for the keratin UFMs. Sorption capacities of keratin UFMs and original keratin feathers were investigated from 200 mL dye solution with commercial dye concentration of 2 g/L at pH 2 for 12 h at 25 °C. Dye removal efficiencies at different pHs (2~6) was measured to determine the optimal condition for dye sorption. Results show pH 2 ensured the highest efficiency. After sorption, dye concentration in water was measured by a UV-vis spectrophotometer (Model DU 720, Beckman Coulter Inc., Brea, CA) at wavelength of maximum absorbance, 595 nm and 543 nm for RB5 and DR80, respectively. Sorption capacity of UFMs was determined by the change of dye concentration in water before and after sorption (See Equation 3).

$$\text{Sorption capacity}(\text{mg/g}) = \frac{(C_0 - C_t)*V}{m} \quad \text{Equation 3}$$

where C_0 and C_t are concentrations of dye in solution before and after sorption (mg/L), respectively. V is the volume of dye solution(L); m is the weight of UFMs used (g).

Dye removal efficiency at each sorption cycle was measured by adding keratin UFMs to a 200 mg L^{-1} aqueous dye solution for 300 min in each sorption (liquor ratio of keratin UFMs to water was 1:2000). Efficiency was determined by Equation 4.

$$\text{Sorption capacity}(\%) = \frac{C_0 - C_t}{C_0} * 100 \quad \text{Equation 4}$$

After one sorption cycle, keratin UFMs were regenerated by immersing the them into 50 mL of 0.1 g L^{-1} NaOH solution with squeeze for 30 min. The regenerated keratin UFMs were used for another sorption study in the subsequent cycles after pH adjustment.

Models of isotherms and kinetics for dye sorption were determined as followings. The Langmuir isotherm model assumes that the sorbate forms a monolayer coverage on a homogeneous sorbent surface, whose linear equation is expressed as Equation 5.

$$[D]_f = \frac{K_L[S]_f[D]_s}{1 + K_L[D]_s} \quad \text{Equation 5}$$

Where $[D]_f$ (mg/g) and $[D]_s$ (mg/L) are the concentrations of dyes in sorbent and water solution at equilibrium, $[S]_f$ is the saturated dye concentration on the sorbent. K_L(L/mg) is the constant for Langmuir isotherm. The Freundlich isotherm model is an empirical formula assumes that multilayer adsorption occurred on a heterogeneous surfaces and non-uniform distribution of adsorption heat over the surface without a saturation of adsorption sites. Its linearized equation is given as Equation 6:

$$\ln[D]_f = \ln K_F + \frac{1}{n}\ln[D]_s \quad \text{Equation 6}$$

where K_F is the Freundlich constant and n is the heterogeneity factor, respectively. The pseudo-first-order model assumes that the rate change of adsorbate uptake with time is directly related to the difference in saturation concentrations, while the pseudo-second-order model assumes that the adsorption rate determining step may be a chemical surface reaction. The pseudo-first-order model follows as Equation 7.

$$\ln\left([D]_f - [D]_{ft}\right) = \ln[D]_s - k_1 t \quad \text{Equation 7}$$

The pseudo-second-order model follows Equation 8:

$$\frac{t}{[D]_{ft}} = \frac{1}{k_2[D]_f^2} + \frac{t}{[D]_f} \quad \text{Equation 8}$$

where k_1 (min^{-1}) and k_2 (mg $g^{-1}min^{-1}$) are rate constants of pseudo-first-order and pseudo-second-order kinetics equations, respectively. $[D]_{ft}$ (mg g^{-1}) is the adsorption capacity at time t.

Removal of organic solvent from water or emulsions

Different concentrations of PAN with molecule weight of 100000 in DMSO (0.025 to 1 wt. %) were prepared. The solution was stirred for 5 min, transferred to coolants at -80 °C for 2 h for freeze-extrusion, and then freeze-dried at -57 °C for 170 h. To have PAN UFMs a stronger organic solvent sorption capacity, bifunctional benzoxazine monomer(Ba) was added to the solution of PAN before freezing. By heating PAN UFMs incorporated with Ba, bifunctional benzoxazine was polymerized to form polybenzoxazine (PBZ).[28] PBZ made the material more hydrophobic and lipophilic, and thus more capable of hydrophobic solvent sorption and emulsion separation.[29] Preparations of Ba-a were described in SI. Polymerization of Ba-a into PBZ are shown in scheme 1.

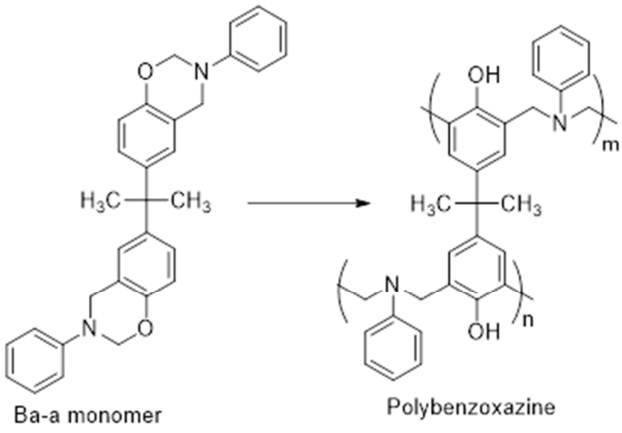

Scheme 1. Illustration showing the synthesis of PBZ by in situ polymerization

PAN UFMs via FDCE were also prepared for comparison with UFMs via freeze-extrusion. UFMs via FDCE were prepared according to method developed by Si et al.[15] Briefly, electrospun PAN fibers were prepared by dissolving PAN (Mw 100,000) and Ba-a (Ratio of PAN to Ba-a was 4:1) into dimethylformamide at concentrations of 7%. The solution was loaded into a syringe and electrospun under a voltage of 25 kV with a distance of 25 cm between the receptor and syringe needle. Different amounts of obtained electrospun membranes were cut into small pieces, and were homogenized in a water/tert-butanol (weight ratio of 4:1) mixture to yield a uniform nanofibre dispersions. The dispersions were frozen in -80 °C for 2h and freeze-dried at -57 °C for 170 h.

Solvent uptake of the PAN UFMs via freeze-extrusion and FDCE from water was measured by immersing the matrices in various solvents from chloroform, mineral oil, hexane and engine oils. To measure separation of engine oil from oil/water emulsion, PAN UFMs via freeze-extrusion were dipped into the emulsion. The matrices were weighed before (W_0) and after (W_t) being taken out from solvent at a certain time without dripping. The solvent uptake ratio was calculated using Equation 9:

$$\text{Solvent uptake} = \frac{W_t - W_0}{W_0} \quad \text{equation 9}$$

Tween 20-stabilized engine oil/water emulsion with an average droplet size of 200 nm was prepared.

Statistical analysis

All the data points were compared using the one-way analysis of variance by the Scheffé test with a confidence interval of 95%. A p value smaller than 0.05 indicated a statistically significant difference. The error bars in the figures represent plus and minors one standard deviation. The data in the figures labelled with different letters indicate their values are significantly different. All statistical analysis was conducted using SAS (SAS Institute Inc., Cary, NC).

Results and discussion

Formation of fibrous matrices between ices

Figure 1 shows the formation of 3-D polymeric matrices during freezing. Basically, there are three stages: Formation of ice crystals, precipitation of polymers between ices and accumulation of polymer precipitates into 3D matrices with the help of ice. Figure 1a shows ice first formed on the wall of a container when the container was surrounded with cooling fluids. However, ices were not simultaneously formed in all areas of walls, or isotherm regions. This is because that heat released from ice formation delayed the formation of ice in the remaining solution around wall of the container. When ice formed, polymers were excluded from ice and concentrated in solution. The concentration of polymer increased gradually as more liquid water turns into ices. When the concentration of polymer exceeded its solubility, polymer precipitated between ices, as shown in Figure 1b. A temperature gradient was formed in the container (from rim to center of the container) and the solution was gradually cooled from wall to center of the container. Ices grew towards the direction of the temperature gradient. The polymer continued its concentration, precipitation and accumulation towards the same direction. In the end, as shown in Figure 1c, the precipitated polymer formed a 3-D matrix and filled the whole container when all liquid water was frozen to ice. Because polymer continued its concentration along the direction of temperature gradient, the concentrations of polymer gradually increased from the rim to the center of the container. Therefore, Figure 1c shows that the shade at center is darker than that at the rim. Figure S1 demonstrates that 3-D fibrous and non-fibrous PVA matrices were formed in different solvents, in which PVA has different solubilities. While ices grew, the width of

spaces between ices decreased and the length of spaces between ices increased along the direction of temperature gradient. After the width of space between ices decreased to fibrous level, polymer precipitated within such space formed fibrous matrices. Polymer formed non-fibrous matrices when gaps between ices was large at the time of polymer precipitation. Solubilities of PVA in water and DMSO at freezing point are 60 g/L (Tager, A. A., et al, 1971) and less than 2 g/L (Data from Gaylord Chemical), respectively. In Figure 2Sa, because of the large solubility in water, PVA did not precipitate till the width of space between ices decreased to fibrous level. Therefore, 3-D fibrous PVA matrix was formed. However, in Figure S1b, because of the small solubility in DMSO, PVA precipitated early while the width of space between ices was still large, resulting in the formation of wide ribbon-like matrix. In addition to the solubility of polymers in different solvents, concentrations of polymers also affected the morphologies of the 3-D matrices. This is mentioned in the following part. Furthermore, because ices formed randomly at isotherm regions, fibers precipitated in gaps between ices showed branched patterns, as shown in Figure S1a.

Scheme of mechanism

The formation mechanism of fibrous matrices by freeze-extrusion is presented in **Figure 2**. The upper part of Figure 2 shows the formation of UFMs via freeze-extrusion: Polymer dissolution, fibers formation between ices, and lyophilization. The lower part shows the detailed process of fibers generation during freezing. Phase I: Ices are initially formed in polymer solution. Width of the gap between ices does not reduce to the fibrous level in this phase. The polymer does not precipitate because its concentration between ices does not reach the solubility; Phase II: polymer precipitates in gaps between ices when the width of gaps reduces to fibrous level. At this time, the concentration of polymer between ices exceeds the solubility because more free water molecules turn into ice. As a result, polymer precipitates into fibers; Phase III: Ices grow towards the direction of temperature gradient, e.g. from rim towards the center of the container. Polymer continues its concentration, precipitation, and accumulation along the direction of the temperature gradient in gaps between ices. Since many independent ices form at isotherm regions randomly, as shown in phase III, branched channels formed between ices. Branched fibers could be formed; Phase IV: When all liquid water turns into ices, formation of UFMs is completed. Appropriate concentration and solubility of polymer could ensure the polymer to precipitate after width of space between ices reduces to fibrous level. Therefore a 3-D fibrous matrix is made.

Validation of mechanism

Macroscopically, Figure S2 shows the alignments of the fibers are controlled by the temperature gradients, which direct the growth of ice, therefore, the fiber matrix. Controllable alignments of fibers in matrix by temperature gradient validate that the polymer continued its concentration, precipitation and accumulation towards temperature gradient. In Figure S2a, when a container was gradually inserted into the cooling fluid, the growth direction of ices was from bottom to top of the cylinder, therefore, the fibers grew from bottom to top, and aligned parallel to each other. When temperature gradient was from rim towards center of a large cylindrical container by immersing a container into the cooling fluid immediately, fibers are aligned toward the center of the container, as shown in Figure S2b. Likewise, all the fibers in the spherical matrices aligned towards the center when the sphere was immersed into the cooling fluid quickly (Figure S2c).

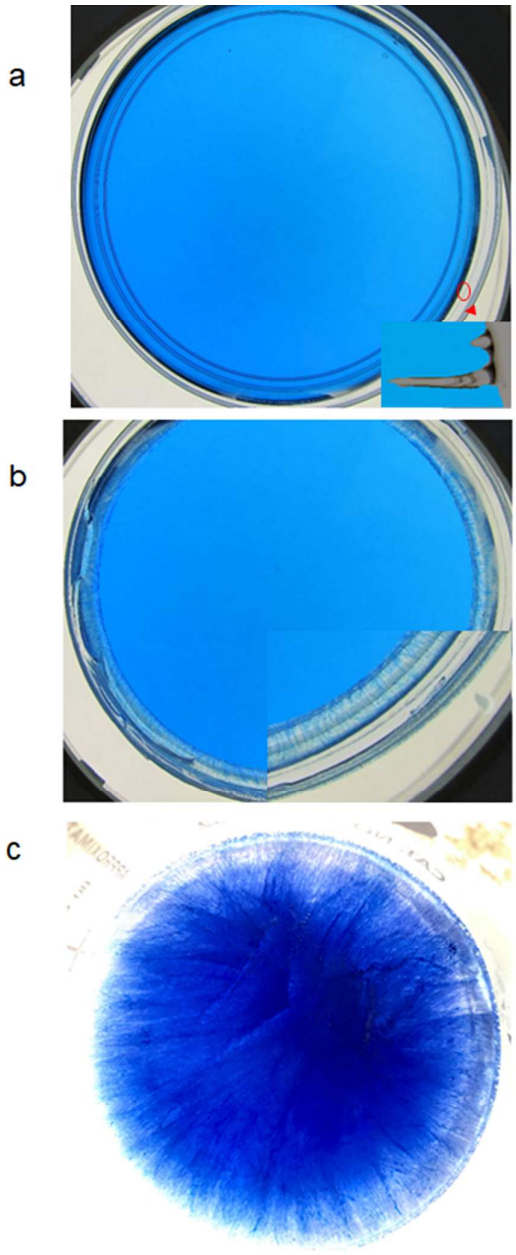

Figure 1. a) Ice formation on the wall of a container (Magnified view on the wall is shown at right corner). b) PVA precipitated between ices (Magnified view at the rim of solution is shown at right corner). c) 3-D PVA matrix formation when all liquid water turned into ice.

Container of RB 19 dyed PVA solution (1 g/L) was dipped into cooling fluid immediately at -80 °C.

Figure 3a shows that the concentration of polymer affects diameters of formed fibers by freeze-extrusion. Results from Figure 3a validate that morphologies of polymer matrices are determined by the width of spaces between ices. Under a high concentration of polymers, changing a small amount of liquid water into ice easily leads to precipitation of polymers between gaps of ices. However, such little amount of water has very limited contribution to the size increase of ices, leading to large width of the gaps between ices. As a result, diameters of fibers are also large. Under a low concertation of polymers, large amount water molecules could turn into ices before the polymer precipitates. Therefore, the size of ices remarkably increases and thus the width of gaps between ices are small. Fibers precipitated in such small gaps have small diameters. Taking keratin for example (Figure 3a), when the protein concentration decreased from 0.1% to 0.025% (w/w), the average fiber diameter decreased from 6.8 µm to 1.8 µm (significantly different with p-value less than 0.0001). It should be noted that concentration of polymer increases along the temperature gradient. Therefore, diameters of formed fibers also increase, leading to large deviation of fiber diameters, as shown in Figure 3a and b.

Figure 3b shows that freezing temperature also affects the fiber radius after freezing. Results from Figure 3b also validate that morphologies of polymer precipitation are determined by the width spaces between ices. Precipitation rate of polymer is slow under high freezing temperature. Lots of unsolidified polymers move along with the temperature gradient. As a result, concentration of polymer at the end of temperature gradient, or solution center, increases, leading to large diameters of formed fibers and small size of UFMs (sizes of UFMs under different temperature are shown in Figure S3). Moreover, at a high freezing rate, the average diameter and number of ices per unit volume decreases and increases, respectively. Such change leads to a narrow space between ices.[24] Therefore, fibers precipitated in the gap had a small diameter. As shown in Figure 3b, the average diameter of PVA fibers in matrices at -20 °C was 3.0 um, while the average of diameter at -80 °C reduced to 1.6 um (significantly different with p-value less than 0.0001). In addition, noted that these polymers have similar solubilities, so under same freezing temperature and polymer concentration, diameters of fibers formed have no significant difference. Alternatively, polymers may be encapsulated in the ice if the rate of freezing is too fast.[20] As a result, amorphous structures are formed under extreme low temperature (-196 °C). SEM of formed materials under -196 °C is shown in Figure S4.

Limited degrees of crystallinity and drawing of formed fibers by freeze-extrusion

Figure 4 shows that fibers via freeze-extrusion have a low degree of crystallinity and drawing. The freeze-extruded fibers in Figure 4 have a degree of crystallinity at 22%, which is lower than that of wet-spun fibers at 44%. During freezing, polymer precipitates at very low temperature. Molecular chains of polymer cannot line up in a regular arrangement at such temperature. Moreover, some ice crystals stay in precipitated polymers and thus hamper interactions among polymer chains. After the sublimation of ices, distance between polymer chains is large, so that interactions between polymer chains are limited.

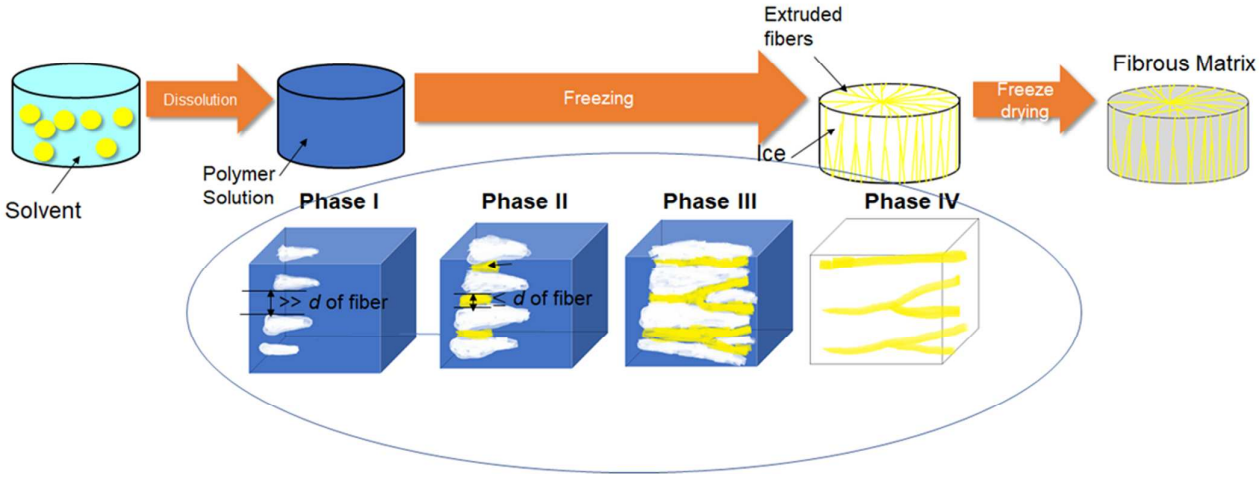

Figure 2. Formation mechanism of fibrous matrices by freeze-extrusion (yellow for polymer, light blue for solvent, dark blue for polymer solution, white for ice). Upper part: Procedures to prepare a 3-D fibrous matrix (in yellow) via freeze-extrusion. Lower part: I, During freezing, ice (in white) forms and grows in polymer solution (in dark blue). II, Polymer precipitates when concentration exceeds the solubility. When a gap between ices (d) decreases to fibrous level, precipitated polymers within the gap have fibrous structure. III, As the

growth of ices from rim to center of the container, precipitated polymer accumulates in gaps between ices. IV When all water turns into ice, fibrous polymer matrices form. Due to random of formation of ice at isotherm regions, fibers in matrices have branches.

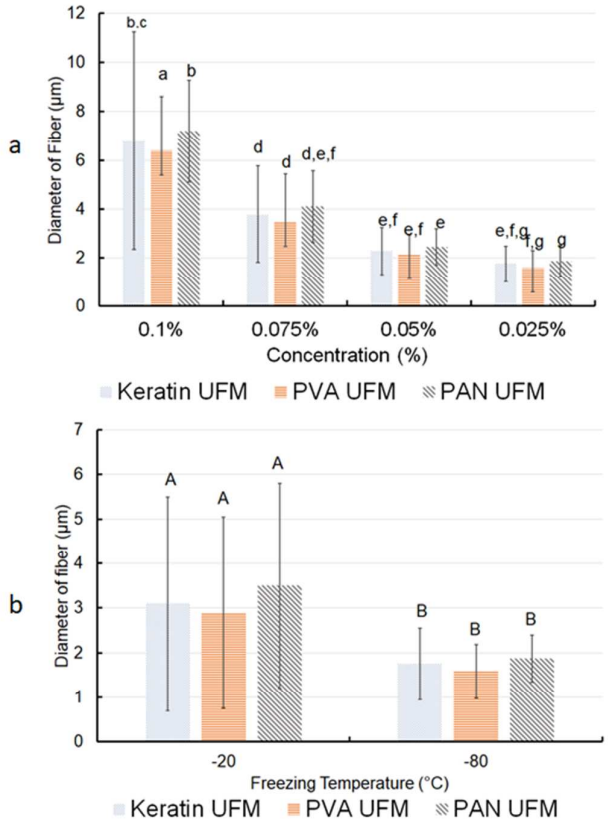

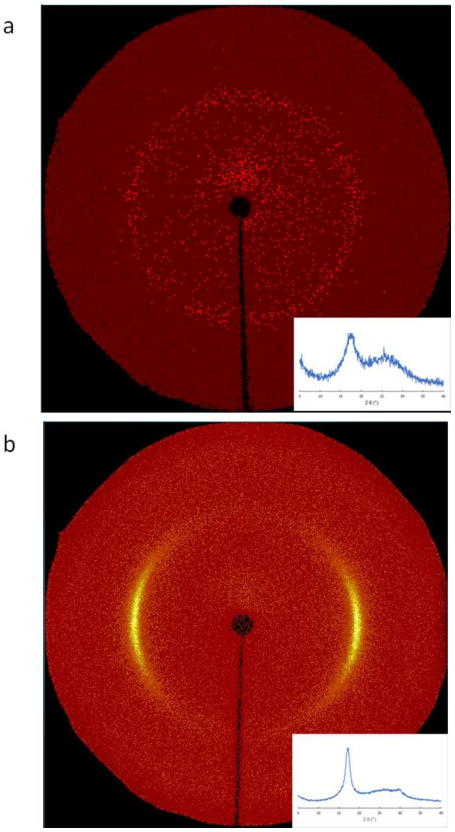

Figure 3. a) High concentration of polymers leads to large diameter of formed fibers via freeze-extrusion. Freezing temperature was -80 ^{o}C b) High freezing rate leads to small radius of formed fibers. Concentration of polymers was 0.025% (w/w).

As a result, degree of crystallinity of fibers via freeze-extrusion is low. Besides the PAN, degrees of crystallinity of PVA and keratin fibers (PVA and keratin) formed via freeze-extrusion were also lower than those of fibers formed by wet-spinning (See Table S1). As for the diffraction rings, unlike wet-spun fibers, freeze-extruded fibers show evenly distributed ring spots, demonstrating very limited degree of drawing, suggesting the low extrusion force exerted by ices. It should be noted that low degree of crystallinity of fibers in matrices did not result from the low degree of drawings. For example, crystallinity of un-drawned PAN film is similar to that of PAN fibers.[30]

Figure 4. Limited degree of crystallinity and drawing of freeze-extruded fibers compared to that of wet-spun fibers. X-ray diffraction patterns and diffractograms of polyacrylonitrile fibers via a) freeze-extrusion and b) wet-spinning. Diffractograms are shown at right corners of images of diffraction patterns.

Durable compressibility of UFMs

PAN was used to investigate and compare the mechanical properties of corresponding UFMs via freeze-extrusion and FDCE. **Figure 5a** shows the compression of UFMs increases with the density. According to the ashby plot of material density versus compression in Figure 5a, the compression stress of freeze-extruded UFMs is better than that of those made by FDCE if the same kind of materials are used at the same density. Figure 5b shows that freeze-extruded UFMs with density of 7.1 mg/cm^3 had satisfactory resiliency. After 100 cycles of compressive fatigue tests, stress loss of UFM was less 4%. Continuous and aligned fibers with branch structures resulted in durable compressibility of UFMs via freeze-extrusion. As a comparison, fibers of UFMs made by FDCE were not aligned and very short. Branched and continuous fibers could offset the effect of low crystallinity. Therefore, comparing to

the matrix via freeze drying of chopped electrospun fibers, matrix via freeze-extrusion have better mechanical properties even though strength of extruded fibers is lower than that of fibers from FDCE because of the difference between crystallinity.

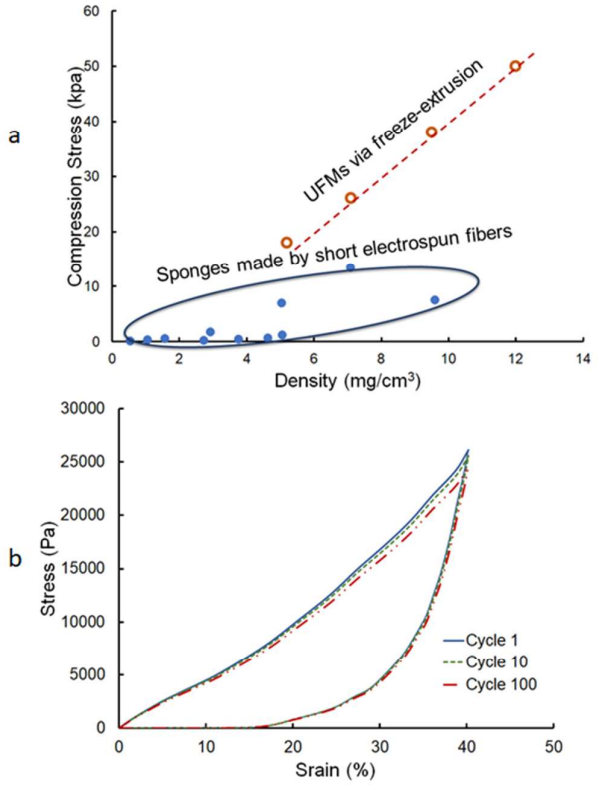

Figure 5. a) Better compression strength of PAN UFMs by this work (in red line) than the other work via FDCE (in blue dot) [15, 31] with different densities; b) 100-cycle compressive fatigue tests with strain (ξ) of 40% on PAN UFMs with density of 7.1 mg/cm^3.

Tunable densities of ultra-light UFMs

UFMs with ultralow densities were developed via freeze-extrusion. Freeze-extruded UFMs with various densities (0.65–12 mg/cm^3) were simply prepared by adjusting the initial concentrations ofpolymer solution. Density of these matrices was as low as 0.65 mg / cm^3 and porosity was up to 99.95%, similar to matrices made by FDCE.[14, 31]

As freeze-extruded fibers, UFMs have some unique features. Compared to electrospun and wet-spun fibers, low degree of crystallinity of freeze-extruded fiber brings about a large portion of amorphous areas in such fibers. Based on large amorphous areas and high porosity, UFMs have high sorption capacity in water treatment. High degree of amorphousness of fibers in UMFs could improve the sorption capacity of pollutants, such as dyes from water. High porosity of UFMs could enhance the solvent sorption from water. UFMs also exhibit highly controlled alignment because fibers were extruded to accumulate along the growth direction of ices. In addition, as ices, fibers have branched structures. Branched structures significantly increase the compressibility of UFMs and reusability in water treatments.

Excellent performance of dye sorption

Figure 6 shows a potential application of freeze-extruded UFMs made of hydrophilic keratin. They were used for dye sorption and sorption recycling. According to previous studies, majority of dyes are sorbed into the internal surfaces rather than external surfaces of fibers in matrices.[32, 33] Therefore, linear densities of fibers do not affect dye sorption much. Alternatively, fibers in matrices via freeze-extrusion may have larger accessible areas for dyes than original fibers. Freeze-extruded keratin fibers (less than 5% degree of crystallinity) had lower degree of crystallinity than keratin feathers (22% degree of crystallinity). As a result, dyes could migrate into internal surfaces of fibers more easily. Moreover, some ice crystals stay in precipitated polymers and thus hamper interactions among polymer chains. After the sublimation of ices, distance between polymer chains is large, so that interactions between polymer chains are limited. As a result, surface area could be dramatically increased. Keratin UMFs have much larger surface area (720 m^2/g) than keratin feather (barbs) itself (176 m^2/g). Based on the results of isotherm of sorption for RB 5 on keratin UFMs and original feather, the dye sorption capacity of UFMs was up to 1200 mg/g while of keratin was 360 mg/g. This shows that sorption of dyes correlates with the surface area. It should be noted diameters of fibers do not affect the overall surface area of UFMs significantly. Sorption of dyes did not change significantly on UMFs with similar surface area and different fiber diameters (See Table S2). Isotherm of DR 80 on keratin UFMs was also measured and these results are in Figure S5 and Table S3. These results also show that Langmuir isotherm was favorable to describe the sorption behavior for both RB5 and DR80, demonstrating that the sorption of RB5 and DR80 on the keratin UMFs was a homogeneous surface with monolayer sorption. Keratin carry positive charges (-NH_3^+) under acidic condition so that dyes could be sorbed to the internal sites of fibers via electrostatic attraction. Kinetic study further validates such sorption mechanism (see Figure S6 and Table S4). Results show that the pseudo-second order model better described the sorption behaviours of RB5 and DR80, suggesting that the sorption of RB5 and DR80 onto keratin UFMs might be chemisorption including valence forces via exchanging of electrons between sorbent and sorbate.

Based on the sorption mechanism, desorption was conducted via converting the electrostatic attraction to electrostatic repulsion between dyes and UFMs. Under alkaline condition, both of keratin UFMs and dyes carry negative charges. Figure 6b shows after 5 times of recycling, efficiency of dye removal was still as high as 84% ($V_{sorption}/V_{desorption}$ = 4). Figure S7 further determined the optimum conditions for both high dye desorption efficiency (%) and high concentration factor (ratio of dye concentration in the eluate over its concentration in the sorption step solution) when varying the volumetric ratio $V_{sorption}/V_{desorption}$ up to 40. The concentration factor increases with the volume ratio of sorption and desorption ($V_{sorption}/V_{desorption}$). When the desortpion efficiency of dye was

higher than 80%, the highest concentration factor could be up to 17. Further increase the $V_{sorption}/V_{desorption}$ could still increase the concentration factor up to 25. However, desorption efficiency decreased to 60%. Besides that, dye removal efficiency with real waste water was also determined. Usually the concentration of total dissolved solids including salts in textile waste water is below 10 g/L[34]. Therefore, we measured dye removal efficiency with salt concentrations from 0 ~ 20 g/L. As shown in Figure S8, the removal efficiency for RB5 and DR80 decreased from around 96% to 85% with the increase of NaCl concentration from 0 to 20 g/L (higher than 90% when NaCl concentration was 10 g/L). This because of the competitive effect between Cl^- and the dye molecules with sorption sites on keratin UFMs. This result shows that keratin UFMs could be applied into dye sorption from real waste water.

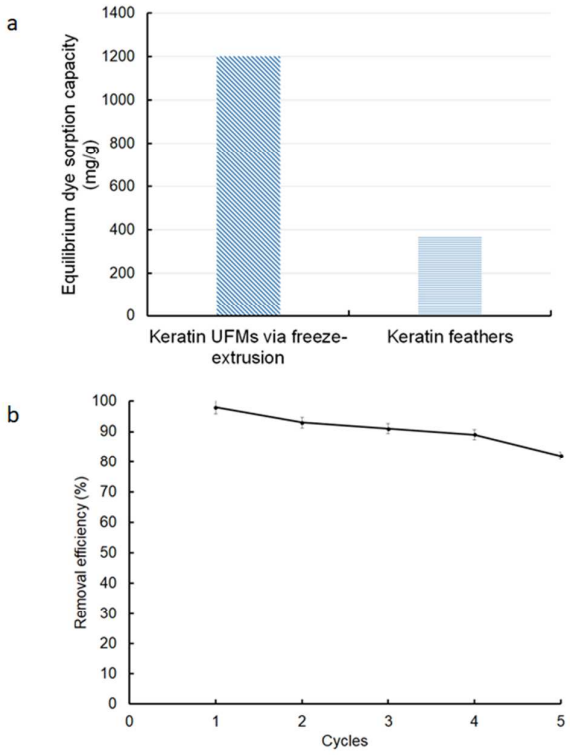

Figure 6. a) Dye sorption capacities of RB5 (having negative charges) at equilibrium using freeze-extruded keratin UFMs and keratin feathers, b) Recycle study of Reactive Black 5 removal using freeze-extruded keratin UFMs. The density of UFMs was 7.2 mg/cm^3 ($V_{sorption}/V_{desorption}$ = 4).

Cost-effective and bio-based materials such as keratin and cellulose have been used as sorbents for dye sorption because they have relative large surface area. These sorbates usually could sorb more dyes than normal materials such as active carbon[35], clay[36] and muds[37]. For example, hen feather and feather-based membrane were used for sorption of various dyes such as congo red[38], tartrazine[39] and CI Reactive Yellow 39[40]. The maximum sorption was under 300 mg/g. Chemically modified feathers were also used as bio-sorbents and demonstrated similar sorption behaviours[41]. Due to the nature of freeze-extrusion, keratin UFMs from freeze-extrusion has significantly higher surface area. Therefore, UFMs demonstrate excellent sorption capacity.

Excellent performance of solvent sorption, emulsion separation and durability

Figure 7a shows the sorption behaviors of freeze-extruded PAN UFMs using different solvents. For PAN UFMs to have a stronger organic solvent sorption capacity, bifunctional benzoxazine monomer(Ba) was added to the solution of PAN before freezing. Details experiments are shown in experimental section. Figure 7a shows matrices with low densities, have strong ability to sorb solvents from water or emulsion. Figure 7b shows a linear relationship between sorption capacities of PAN UFMs and densities of solvent, indicating similar hydrophobic interaction of PAN UMFs with all hydrophobic solvents. Higher densities of solvents were, larger weight UFMs sorbed. It was found that pores formed by the interconnection of fibers were 20~40 μm and there is no significant difference in pore size among UFMs with different densities (2~9 mg/cm^3). Porosity should be a major factor affecting solvent sorption. Figure 7c demonstrates excellent sorption ability of PAN UFMs resulted from their large porosity. Figure 7c shows a linear relationship between porosity of PAN UFMs and solvent sorption capacity. Larger porosity, or lower density of PAN UFMs, larger sorption capacity of solvents. The porosity of matrix per unit mass increased from 91.3 m^3/g to 411 m^3/g, and the solvent adsorption increased from 7000% to 34000%. Figure 7d shows better reusability of PAN UFMs via freeze-extrusion than that via FDCE in solvent sorption. Because of similar pore size and porosity, matrices from freeze-extrusion and FDCE have similar sorption capacity. However, upon 50 sorption–squeeze-evaporation cycles, sizes of PAN UFMs from FDCE decreased by around 50%, and therefore had lower sorption capacities for solvent. Due to good mechanical properties of PAN UFMs via freeze-extrusion, size and porosity of such UFMs remained the same even after 50 sorption cycles. In Fig, 7d, sorption of chloroform with UFMs via freeze-extrusion did not change significantly even after 50 times of reuses while sorption capacity for UFMs from FDCE decreased by around 50% after 50 times of reuses. Freeze-extrusion is a relative simple way to fabric materials with low densities and high porosity. These properties are crucial for high sorption capacity of organic solvent. Porosity of UFMs is comparable with current ultralight materials such as cellulose nanofibril aerogels[42], carbon nanotube sponges[43, 44] and short electrospun fibers in colloidal dispersions[31]. Therefore, similar capacity of solvent sorption could be obtained using UFMs and other materials with similar porosity.

Figure 7e shows separation of oil/water emulsion using freeze-extruded PAN UFMs incorporated with Ba. Only oil penetrated the PAN UFMs because of high hydrophobicity of PAN UFMs. Phase I in Figure 7e shows a piece of PAN UFMs immerged in oil/water emulsion. After sorption, as shown in phase II of Figure 7e, PAN UFMs sorbed all oil, turning the emulsion transparent. Phase III of Figure 7e shows that PAN UFMs selectively removed oil from oil/water emulsions. As shown in the Figure 7e, pure oil was squeezed out of PAN UFMs at the end of the sorption.

Conclusions

In this paper, the mechanism of UFMs made by freeze-extrusion is studied. 3-D UFMs are formed though successive polymer precipitation, concentration and accumulation within gaps between ices during freezing. Based on formation of ice and precipitation of polymers between ices, effects of polymer concentrations, solvents and freezing rates on the morphology of UFMs is thoroughly studied. Unique phenomena of UFMs via freeze-extrusion, such as size changes of UFMs caused by freezing rate, morphologies changes of UFMs using different solvents, increase of density of fibrous matrices and diameter of fibers in matrices along the temperature gradient could be fully explained by the mechanism this paper develops. Large areas of amorphousness in fibers and high porosity of UFMs ensure such matrices to have a good performance in water treatment and noise absorption. Fibers in freeze-extruded UFMs are continuous, branched and alignment controlled, giving UFMs good durability. Freeze-extruded UFMs are easy to prepare, with wide range of available polymers and solvents according to specific application needs.

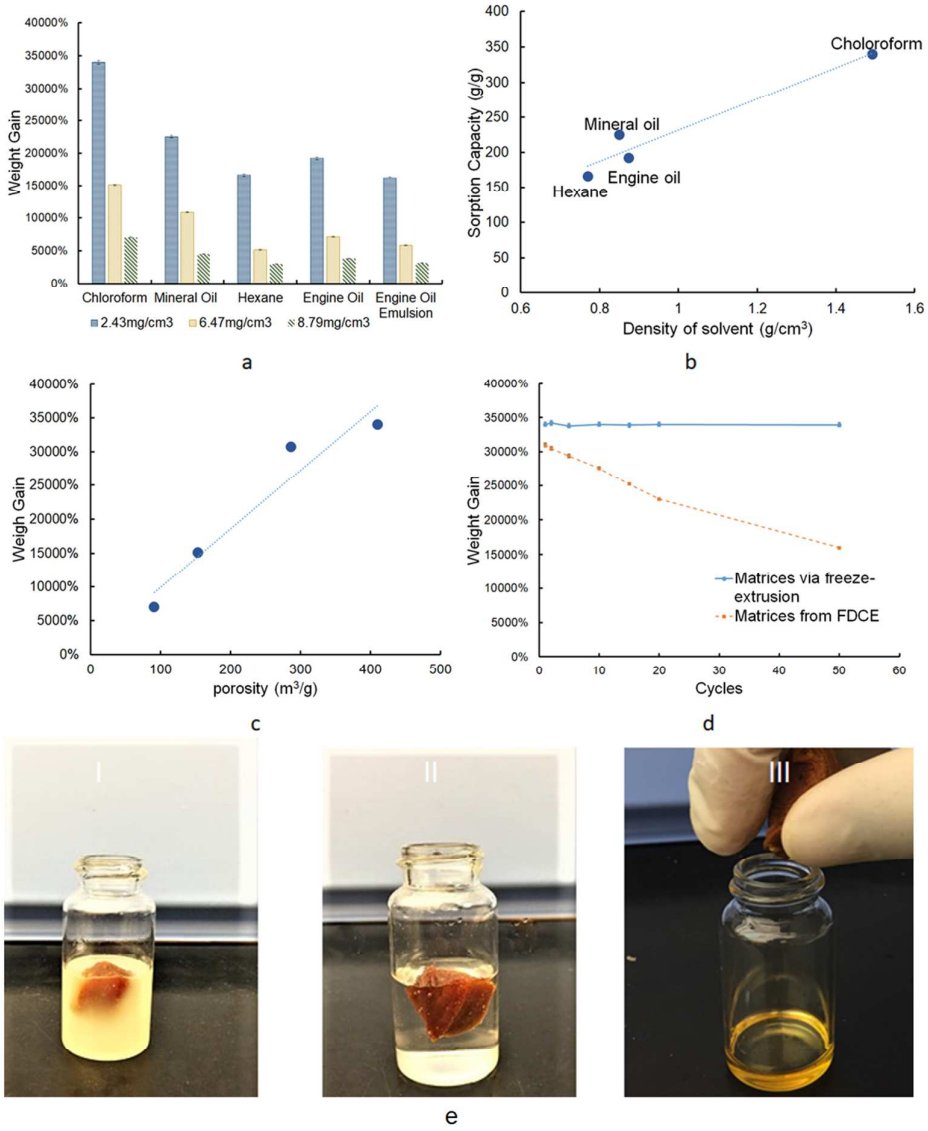

Figure 7. a) Uptakes of hydrophobic liquids in wt.% from water or emulsions as function densities of PAN UFMs incorporated with Ba-a, b) Linear relationship between sorption capacities of PAN UFMs incorporated with Ba-a (density was 2.43 mg/cm^3) and densities of sorbed solvents, c) Linear relationship between porosity of PAN UFMs incorporated with Ba-a and weight gain after sorption (solvent was chloroform), d) Comparison of chloroform uptake of PAN UFMs incorporated with Ba-a made by freeze-extrusion (density 2.43 mg/cm^3)

and FDCE (density 3.49 mg/cm^3) at different reuse cycles. UFMs were squeezed and solvent was evaporated after each cycle of sorption. e) Engine oil separation from water/oil emulsions using freeze-extruded PAN UFMs incorporated with Ba-a (density was 8.79 mg/cm3). I) PAN UFMs put into emulsion, II) all yellowish oil sorbed into matrices leaving emulsion only water. III) only oil in the emulsion removed by PAN UFMs and reuse of PAN UFMs by squeezing.

Conflicts of interest

The authors declare no conflict of interest.

Acknowledgements

This research was financially supported by National Institute of Food and Agriculture [Multi-State Project S1054 (NEB 37–037)], USDA Hatch Act, and the Agricultural Research Division at the University of Nebraska-Lincoln, USA. Bingnan Mu and Wei Li are grateful to the John and Louise Skala Fellowship and AATCC Students Grant for financial support. The research was performed in part in the Nebraska Nanoscale Facility: National Nanotechnology Coordinated Infrastructure and the Nebraska Center for Materials and Nanoscience, which are supported by the National Science Foundation under Award ECCS: 1542182, and the Nebraska Research Initiative.

Notes and references

1. S. N. Schiffres, K. H. Kim, L. Hu, A. J. McGaughey, M. F. Islam and J. A. Malen, *Advanced Functional Materials*, 2012, **22**, 5251-5258.
2. T. Bravo and C. Maury, *Journal of Sound and Vibration*, 2018, **417**, 165-181.
3. L. Zang, J. Ma, D. Lv, Q. Liu, W. Jiao and P. Wang, *Journal of Materials Chemistry A*, 2017, **5**, 19398-19405.
4. C.-T. Wang, C.-L. Wu, I.-C. Chen and Y.-H. Huang, *Sensors and Actuators B: Chemical*, 2005, **107**, 402-410.
5. M. Y. Baktash and H. Bagheri, *Journal of Chromatography A*, 2017, **1500**, 69-75.
6. N. T. Hung, A. R. Nugraha and R. Saito, *Carbon*, 2017, **118**, 278-284.
7. Y. Kosaki, H. Izawa, S. Ishihara, K. Kawakami, M. Sumita, Y. Tateyama, Q. Ji, V. Krishnan, S. Hishita and Y. Yamauchi, *ACS applied materials & interfaces*, 2013, **5**, 2930-2934.
8. S. Piotto, L. Sessa, L. Baldino, S. Cardea and E. Reverchon, in *Advances in Bionanomaterials*, Springer, 2018, pp. 75-84.
9. B. Duan, C. Dong, X. Yuan and K. Yao, *Journal of Biomaterials Science, Polymer Edition*, 2004, **15**, 797-811.
10. Y. Q. Wan, J. H. He, J. Y. Yu and Y. Wu, *Journal of applied polymer science*, 2007, **103**, 3840-3843.
11. S. Cai, H. Xu, Q. Jiang and Y. Yang, *Langmuir*, 2013, **29**, 2311-2318.
12. H. Xu, S. Cai, L. Xu and Y. Yang, *Langmuir*, 2014, **30**, 8461-8470.
13. H. Xu, S. Cai, A. Sellers and Y. Yang, *RSC Advances*, 2014, **4**, 15451-15457.
14. W. Teo, S. Liao, C. Chan and S. Ramakrishna, *Current Nanoscience*, 2008, **4**, 361-369.
15. Y. Si, J. Yu, X. Tang, J. Ge and B. Ding, *Nature communications*, 2014, **5**, 5802.
16. X. Liu, L. Smith, G. Wei, Y. Won and P. X. Ma, *Journal of biomedical nanotechnology*, 2005, **1**, 54-60.
17. P. X. Ma and R. Zhang, 1999.
18. L. Qian and H. Zhang, *Green Chemistry*, 2010, **12**, 1207-1214.
19. W. Mahler and M. F. Bechtold, *Nature*, 1980, **285**, 27-28.
20. H. Zhang and A. I. Cooper, *Advanced materials*, 2007, **19**, 1529-1533.
21. L. Qian, A. Ahmed, A. Foster, S. P. Rannard, A. I. Cooper and H. Zhang, *Journal of Materials Chemistry*, 2009, **19**, 5212-5219.
22. L. Qian, E. Willneff and H. Zhang, *Chemical Communications*, 2009, 3946-3948.
23. Q. Jiang, H. Xu, S. Cai and Y. Yang, *Journal of Materials Science: Materials in Medicine*, 2014, **25**, 1789-1800.
24. S. Deville, E. Saiz, R. K. Nalla and A. P. Tomsia, *Science*, 2006, **311**, 515-518.
25. L. Qian and H. Zhang, *Journal of chemical technology and biotechnology*, 2011, **86**, 172-184.
26. J. Santamarina, K. Klein, Y. Wang and E. Prencke, *Canadian Geotechnical Journal*, 2002, **39**, 233-241.
27. H. Xu and Y. Yang, *ACS Sustainable Chemistry & Engineering*, 2014, **2**, 1404-1410.
28. N. Ghosh, B. Kiskan and Y. Yagci, *Progress in polymer Science*, 2007, **32**, 1344-1391.
29. Y. Si, T. Ren, Y. Li, B. Ding and J. Yu, *Carbon*, 2012, **50**, 5176-5185.
30. H. Guo, T. Sreekumar, T. Liu, M. Minus and S. Kumar, *Polymer*, 2005, **46**, 3001-3005.
31. G. Duan, S. Jiang, V. Jérôme, J. H. Wendorff, A. Fathi, J. Uhm, V. Altstädt, M. Herling, J. Breu and R. Freitag, *Advanced Functional Materials*, 2015, **25**, 2850-2856.
32. E. Guibal, C. Milot and J. M. Tobin, *Industrial & Engineering Chemistry Research*, 1998, **37**, 1454-1463.
33. C. H. Giles, A. P. Montgomery and A. H. Tolia, *Textile Research Journal*, 1962, **32**, 99-107.
34. A. Al-Kdasi, A. Idris, K. Saed and C. T. Guan, *Global nest: the Int. J*, 2004, **6**, 222-230.
35. T. Maneerung, J. Liew, Y. Dai, S. Kawi, C. Chong and C.-H. Wang, *Bioresource technology*, 2016, **200**, 350-359.
36. Y. Ho and C. Chiang, *Adsorption*, 2001, **7**, 139-147.
37. G. Ratnamala, K. V. Shetty and G. Srinikethan, *Water, Air, & Soil Pollution*, 2012, **223**, 6187-6199.
38. A. Mittal, V. Thakur, J. Mittal and H. Vardhan, *Desalination and Water Treatment*, 2014, **52**, 227-237.
39. A. Mittal, L. Kurup and J. Mittal, *Journal of hazardous materials*, 2007, **146**, 243-248.
40. O. M. Freitas, L. M. Moura, S. A. Figueiredo and M. T. Pessoa de Amorim, *Coloration Technology*, 2016, **132**, 421-430.
41. M. A. Khosa, J. Wu and A. Ullah, *Rsc Advances*, 2013, **3**, 20800-20810.

42. F. Jiang and Y.-L. Hsieh, *Journal of Materials Chemistry A*, 2014, **2**, 6337-6342.
43. X. Gui, J. Wei, K. Wang, A. Cao, H. Zhu, Y. Jia, Q. Shu and D. Wu, *Advanced materials*, 2010, **22**, 617-621.
44. Q. Peng, Y. Li, X. He, X. Gui, Y. Shang, C. Wang, C. Wang, W. Zhao, S. Du and E. Shi, *Advanced Materials*, 2014, **26**, 3241-3247.

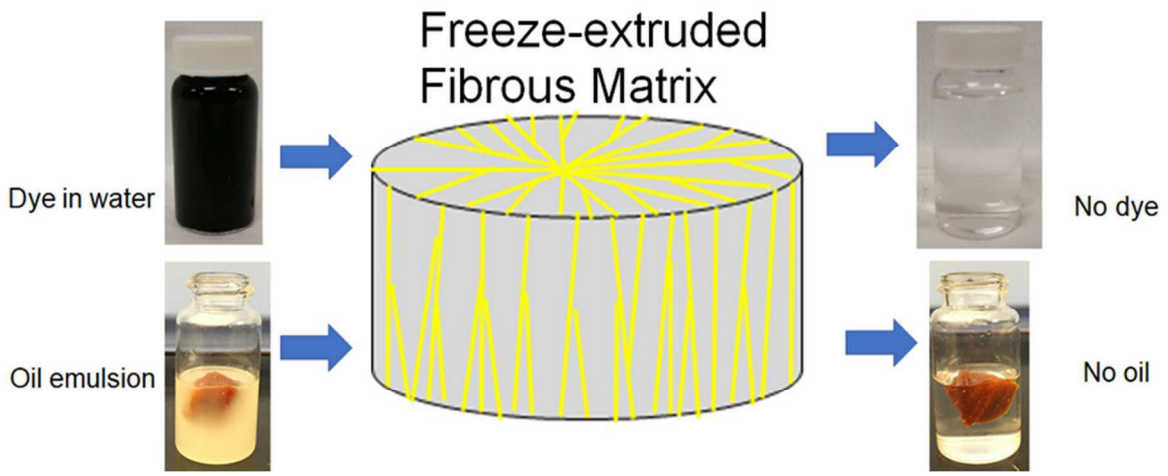

High amorphousness, large porosity and good mechanical properties endow fibrous matrices with high sorption ability and reusability.